J Mater Sci (2009) 44:186–197
DOI 10.1007/s10853-008-3103-2

Effect of chromium content on the microstructure and mechanical properties of multipass MMA, low alloy steel weld metal

M. H. Avazkonandeh-Gharavol · M. Haddad-Sabzevar · A. Haerian

Received: 11 June 2008 / Accepted: 4 November 2008 / Published online: 27 November 2008

Abstract Effect of chromium content in the range of 0.05–0.91 wt% on the microstructure and mechanical properties of Cr–Ni–Cu low alloy steel weld metal was investigated. All welds were prepared by manual metal arc welding technique in flat position. Microstructure of the welds was examined by optical and scanning electron microscope in both columnar and reheated regions of the weld metal. The results showed increase in acicular ferrite and microphases formed at the expense of primary ferrite and ferrite with second phase with steady refinement of microstructure. According to these microstructural changes, yield and ultimate tensile stresses, Hardness and Charpy V-Notch impact toughness increased, whereas elongation decreased. Increase in Charpy impact value is thought to be due to fine dispersed spheroidized dark microphases at high chromium contents.

Introduction

Mechanical properties of welds are determined by chemical composition, cooling rate (technological parameters such as voltage and current), and microstructure. Microstructure is in fact a function of other variables. The most important factor determining weld metal properties is chemical composition. To achieve optimal combination of strength and toughness for offshore constructions and line piping, new grades of steels such as high strength low alloy steels have been designed and developed. These alloys have a microstructure composed of predominantly acicular ferrite (AF) that insures weldability of low alloy steels and acceptable mechanical properties of the weld metal. Microstructure of weld metal has been, and still is the subject of broad investigations as reported by previous researchers [1, 2]—and now has found its way in welding textbooks [3].

Due to low percentage of solutes in low alloy steels, the weld metal begins to solidify by epitaxial growth of columnar delta-ferrite (δ-ferrite) from the hot-grain structure of the parent plate at the fusion boundary. Therefore, the structure of the parent plate can affect the microstructure, and consequently, mechanical properties of the weld, especially in the case of high heat input welding [4]. The δ-ferrite undergoes a solid-state transformation to austenite as the temperature decreases. The austenite nucleates at the δ–δ grain boundaries and develops into a columnar grain structure that strongly resembles that of the original δ-grains. Bhadeshia et al. claim that the structure of austenite grains can be represented by a space-filling hexagonal prism with length c and cross sectional side length a, where $c \gg a$ [5]. The grains are typically about 100 μm wide and 5000 μm long [6].

Microstructure of low alloy steels are complex and consist of different morphologies of ferrite (including allotriomorph ferrite, ferrite side plates and acicular ferrite), bainite, microphases and some inclusions. Microphase is a collective term for small fractions of martensite, degenerated pearlite, and retained austenite that develops from saturated austenite in the latest stage of transformation. Solid state transformation from austenite to different ferrites occurs in the temperature range of 800–300 °C as explained here under:

M. H. Avazkonandeh-Gharavol · M. Haddad-Sabzevar (✉)
Department of Materials Science and Metallurgy, Faculty of Engineering, Ferdowsi University of Mashhad, Azadi Square, P.O. Box 91775-1111, Mashhad, Iran
e-mail: haddadm@ferdowsi.um.ac.ir

A. Haerian
Sadjad Institute of Higher Education, Mashhad, Iran

Allotriomorphic ferrite (α) is the first phase to form upon cooling of austenite. It nucleates at the columnar austenite grain boundaries and then these grain boundaries become decorated with thin, continuous layers of ferrite. The layers then grow at a rate controlled by the diffusion of carbon. The rate decreases with increasing thickness. This phase is deleterious to toughness because of its low resistance to cleavage crack propagation [7]. Upon further cooling, Widmanstätten ferrite forms. It grows by a displacive mechanism from grain boundary ferrite or bare austenite grain boundaries. Although substitutional solutes and iron atoms do not diffuse during the growth of Widmanstätten ferrite, carbon does partition during transformation. Because of its plate shape, much of the carbon can be accommodated at the sides of the growing plate, so that the plate tip always encounters fresh austenite. Widmanstätten ferrite plates, therefore, elongate at a constant rate and much faster than allotriomorph ferrite.

When all grain boundaries were occupied, intra-granular inclusion-assisted nucleation and growth of AF occurs with a displacive mechanism. Because of the small effective grain size with high angle boundaries, high density of dislocations and chaotic structure, AF is generally accepted for achieving both strength and good toughness. Therefore, the mechanisms and factors affecting nucleation and growth of AF have been extensively studied, and nowadays are still being studied to make the AF as the predominant constituent in the microstructure of welded and wrought alloys [8–10].

Within a multipass weld, the individual weld beads contain a columnar region with the microstructure as described above, and a reheated region that can be subdivided into two regions. The first zone is coarse-grained reheated zone (CGRZ) with grain boundary ferrite nucleated at equiaxed primary austenite grain boundaries, plus intragranular products. The austenite grains in this zone are much smaller than those of the columnar zone. The second zone is fine-grained reheated zone (FGRZ) which consists of fine-grained equiaxed ferrite along with grain boundary second phases.

Effect of chromium on microstructure and properties of a number of grades of steels in various welding techniques are discussed elsewhere [11–13]. In all the cases reviewed earlier, it has been shown that chromium increases tensile properties and hardness, but reduces impact toughness. Loss of toughness has been related to the microphases, martensite–austenite constituents (MAC) for single pass welding, and the percentage of reheated regions in the vicinity of notch in Charpy specimens in multipass welds [11].

The aim of this research is to identify effect of ferro-chromium additions in the coating of electrodes on the microstructure and mechanical properties of Cr–Ni–Cu steel weld metal deposits. Tensile properties and Charpy impact toughness were selected for our assessment. The microstructural study was focused on how chromium additions affect

- the proportion of different regions (columnar, CGR and FGR zones),
- fraction of microstructural constituents in columnar and CGR zones,
- primary austenite grain size in columnar and CGR zones,
- nature of microphases especially in reheated beads, and
- volume fraction, distribution, and chemistry of nonmetallic inclusions.

Experimental procedure

Three high cellulose experimental electrodes (E8010G base) were designed. The ferro-chromium (Fe–Cr) content in the coating was varied such that final weld metal consists of 0.05, 0.53, and 0.91 wt% chromium. The amounts of chromium of Fe–Cr was about 75–80 wt%. The core wire had a diameter of 5 mm, and coating factor was 1.432 in all the electrodes. A constant current power source with DCEP polarity was used in all the cases.

With each of the three electrodes, two all-weld metal coupons were welded according to ANSI/AWS A5.5-96 [14] using a DIN ST52 base. Chemical compositions of consumables and weld assemblies are presented in Table 1 and Fig. 1, respectively. Welding was performed in flat position. The groove was filled with eight layers, each containing two beads, reversing welding direction after each bead. Weld bead geometry is shown schematically in Fig. 2. Welding parameters used in this investigation are indicated in Table 2.

The overall chemical composition of the all-weld metal was determined by conventional quantometery techniques using a Horiba Metalys machine. However, carbon and sulfur were measured by a Horiba C/S analyzer EMIA 220V, and oxygen and nitrogen were determined by LECO TC-436-AR analyzer. From each pair of coupons welded by an electrode designation, one coupon was used to make one tensile specimen, four Charpy impact specimens, and a transverse cross section for metallography. From the other coupon, two tensile specimens and a transverse cross section for metallography were produced.

Metallographic examinations were carried out after etching with 2% Nital in both as-deposited and reheated beads, using optical microscope and LEO 1450VP SEM equipped with an Oxford 7353 EDS. To accentuate the microphases, a selective Beraha tint etch (16 g $Na_2S_2O_3 \cdot 5H_2O$ + 3 g $K_2S_2O_5$ + 94 mL H_2O) was employed. For

Table 1 Chemical composition of consumables

Elements	C	Si	Mn	P[a]	S[a]	Cu	Cr	Ni	Mo[a]	Al[a]	Ti[a]	O[a]	N[a]
Base metal	0.16	0.26	1.44	140	75.76	0.04	0.03	0.07	31.32	100	83.57	137	57
Core wire	0.08	0.03	0.60	85.03	200	0.14	0.02	0.03	300	56.76	–	247	55

[a] These compositions are in ppmw

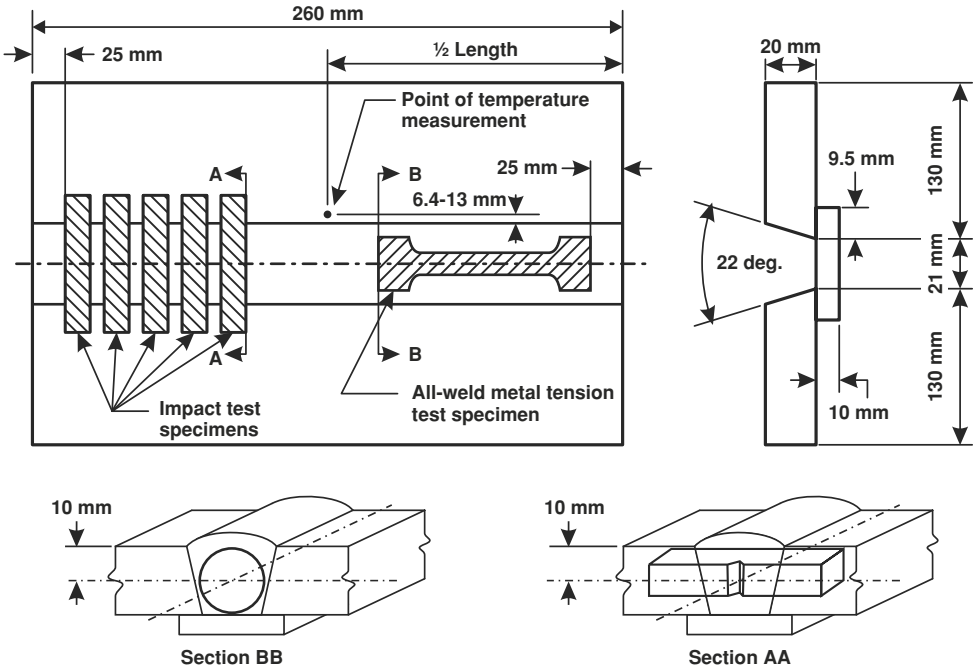

Fig. 1 Weld assembly (*top*) and the location of Charpy and tensile specimens (*bottom*)

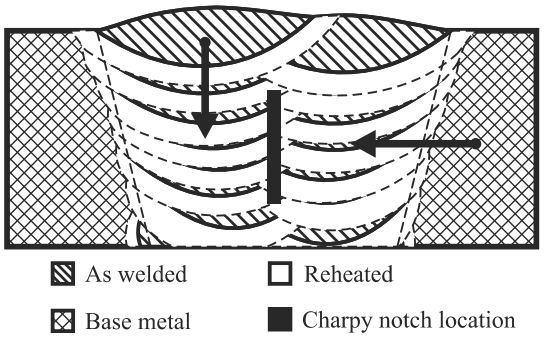

Fig. 2 Weld bead geometry scheme, showing notch location of Charpy specimens and location of hardness survey (arrows)

better results, specimens were pre-etched for 2-s with 2% Nital. Percentage of microstructural constituents in both columnar and CGR zones were determined at 500×. Microphases calculations were carried out at 1000×. Size of primary austenite grains in both columnar and CGR zones were determined at 100×. The volume fraction and size distribution of nonmetallic inclusion were determined on polished surfaces by SEM at 20 kV with 4000× magnification in backscattered mode. In each specimen, ten fields containing a minimum of 570 inclusions were examined.

Tensile properties were determined at room temperature after hydrogen removal treatment at 95–105 °C for 48 ± 2 h using a Zwick Z250 machine. Impact tests were performed at −29 °C with an Avery Denison 300J × 2J machine. Vickers microhardness profiles were produced using a Buehler high quality microhardness tester with 1-kg load. Measurement was done on polished specimens in the top-down direction starting from the top bead with 0.25 mm steps between consecutive measurements. Locations of hardness indentations are shown in Fig. 2. A horizontal hardness profile for specimen containing 0.53 wt% Cr, from base to weld metal (see Fig. 2), under the same conditions was also prepared.

Results and discussion

Chemical composition

Chemical composition analysis of the all-weld metal as a function of Fe–Cr content in the coating is represented in Table 3. Here, a steady increase in Cr content of the weld metal is observed, while other elements remain almost constant. Comparison of data in Tables 1 and 3, shows that

Table 2 Welding parameters used in experiments

wt% Cr in weld metal	Number of run	Welding parameter				
		Current[a] (A)	Voltage[a] (V)	Heat Input[a] (kJ/mm)	Moisture[b] (wt%)	Interpass temperature (°C)
0.05	1	186	29	2.43	2.92	185
	2	185	29	2.45	4.76	185
0.53	1	185	30.5	2.81	2.45	185
0.91	1	186	30.5	2.42	3.19	185
	2	186	30	2.43	4.49	185

[a] Average value per pass

[b] The moisture of electrode coating that determined by standard method described in ANSI/AWS A5.5-96

Table 3 Chemical composition of all-weld metal

Fe–Cr in coating	wt% in weld metal												
	C	Si	Mn	P	S	Cu	Cr	Ni	Mo	Al[a]	Ti	O[a]	N[a]
0.0	0.168	0.35	0.80	0.01	0.015	0.57	0.05	0.17	0.02	5.07	0.022	531	181
4.5	0.163	0.37	0.81	0.01	0.015	0.53	0.53	0.16	0.03	2.33	0.021	577	139
8.0	0.167	0.37	0.80	0.01	0.015	0.56	0.91	0.17	0.02	9.82	0.019	557.5	199.5

[a] These compositions are in ppmw

the level of oxygen and nitrogen of the weld metal are much higher than those of consumables. These elevated levels of oxygen and nitrogen are possibly because of atmospheric contamination and/or chemical reactions of flux ingredients in the weld pool. Variation of oxygen concentration does not affect weld chemistry or properties in this study, and remains fairly constant. It is a well-known fact that the affinity of chromium for oxygen is much less than that of silicon or manganese, and therefore, variation of chromium content does not alter the oxygen concentration in weld metal. It is also evident that chromium has no profound effect on the recovery of other elements.

Metallographic examination

Proportion of different regions

Examination of proportion of different regions of weld metal, i.e., columnar, CGR, and FGR zones, were carried out at the notch location. Study on Charpy notch location revealed that for low levels of chromium, only FGRZ could be distinguished. Increasing Cr content increases fraction of other regions, especially CGRZ. For maximum Cr level small amounts of columnar zone were also observed. Because chromium increases $\gamma \rightarrow \alpha$ transformation temperature, one expects that increase in Cr content would increase fraction of columnar zone as reported by Surian and De-Vedia [13]. Fraction of different zones also depends on heat input level. Because our experimental electrodes were cellulose based, in this study, heat input was higher as compared to those in similar studies. The cellulose in the coating burns during welding and results in an increase in heat input. Therefore, true values of heat input are expected to be somewhat higher than those presented in Table 2. Increase in heat input also results in increase in the area of reheated regions. As a result of this, the fraction of columnar zone becomes negligible.

Columnar microstructure of the last bead

Figure 3 shows the optical and SEM micrographs of weld metal microstructures corresponding to the two extreme Cr concentrations. Results of quantitative metallography are presented in Table 4. Microstructure is subdivided into three microstructural constituents: (1) primary ferrite (PF) that includes both grain boundary and intragranular polygonal ferrite, (2) ferrite with second phase (FS) that contains all the grain boundary-nucleated lath-like morphologies of ferrite, and (3) intragranular Acicular ferrite (AF).

It is evident that there is a steady increase in the percentage of AF with increasing the Cr content of the weld metal at the expense of other constituents. This effect is more pronounced on FS. It is also evident that the microstructure generally becomes finer with increasing Cr content. SEM images (Fig. 3c, f), clearly show that chromium additions greatly refine AF grains.

To suppress allotriomorphic ferrite growth with increase in substitutional alloying elements (like chromium) in isothermal transformations, several mechanisms have been proposed [15]. Amongst these, solute drag-like effect is more likely to occur [15, 16] in both cases of isothermal transformation and welding. Interphase boundary carbide

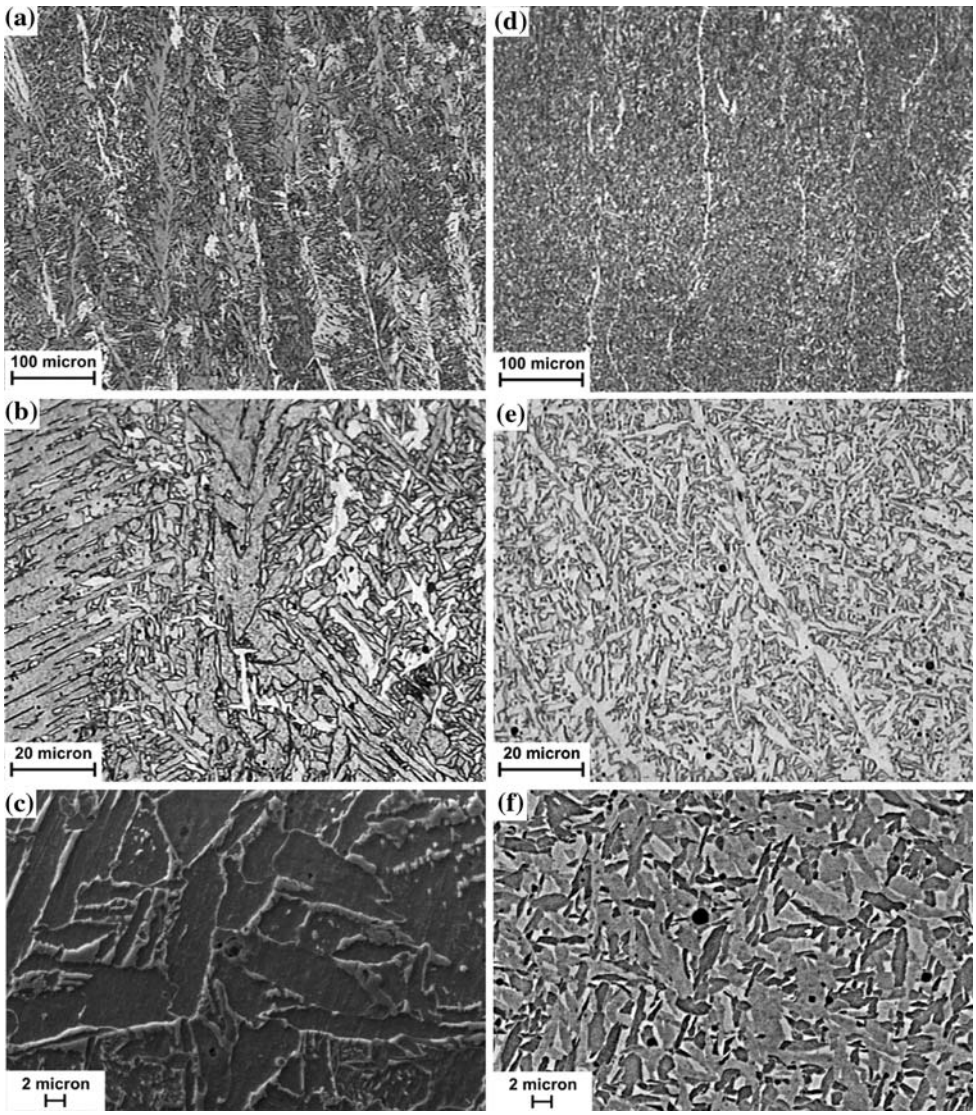

Fig. 3 Optical and SEM micrographs showing microstructural changes in top bead, **a**–**c**, 0.05 and **d**–**f**, 0.91 wt% Cr concentration in different magnifications, **c** secondary, and **f** backscattered SEM micrographs

Table 4 Results of quantitative metallography in columnar and CGR zones of the last bead

Cr (wt%)	Top bead (%)			$\bar{L}$ (μm)[a]	CGRZ (%)			$\bar{l}$ (μm)[a]
	PF	FS	AF		PF	FS	AF	
0.05[b]	24.6	22	47.6	70.19	32.8	17.5	35.5	92.07
0.53	22.8	7.9	69.3	58.20	38.1	13.3	48.6	60.24
0.91	8.9	1.9	89.2	56.64	20.7	12.2	67.1	46.55

[a] The terms $\bar{L}$, $\bar{l}$ stand for mean primary austenite columnar grain width and mean primary austenite grain size in CGRZ, respectively

[b] The sum of microstructural constituents is not 100% in the case of 0.05 wt% Cr, because of existence of a fourth constituent that did not occur in other cases and could not be identified. Volume fraction of this unknown phase is 5.8 and 14.2% in top bead and CGRZ, respectively

precipitation that may be active in the case of welding [2, 7] has not been reported in isothermal transformation [17]. The reason for the decreased FS volume fraction of the weld having displacive mechanism is the increased hardenability with increasing Cr content. It has been proposed that a degree of hardenability is needed for achieving an AF microstructure [18, 19].

Table 4 shows a general decrease in primary austenite grain size in both columnar and CGRZ. This is a direct result of solute drag-like effect of chromium. This effect seems to increase the desired locations for grain boundary products like GBF and FS. However, the experimental results show that AF can develop effectively in the microstructure when the hardenability of the alloy is at acceptable level.

Reheated microstructure

Variation of microstructure in reheated beads was studied in reheated regions produced by the last bead. Microstructures of CGRZ and FGRZ for two extreme Cr contents

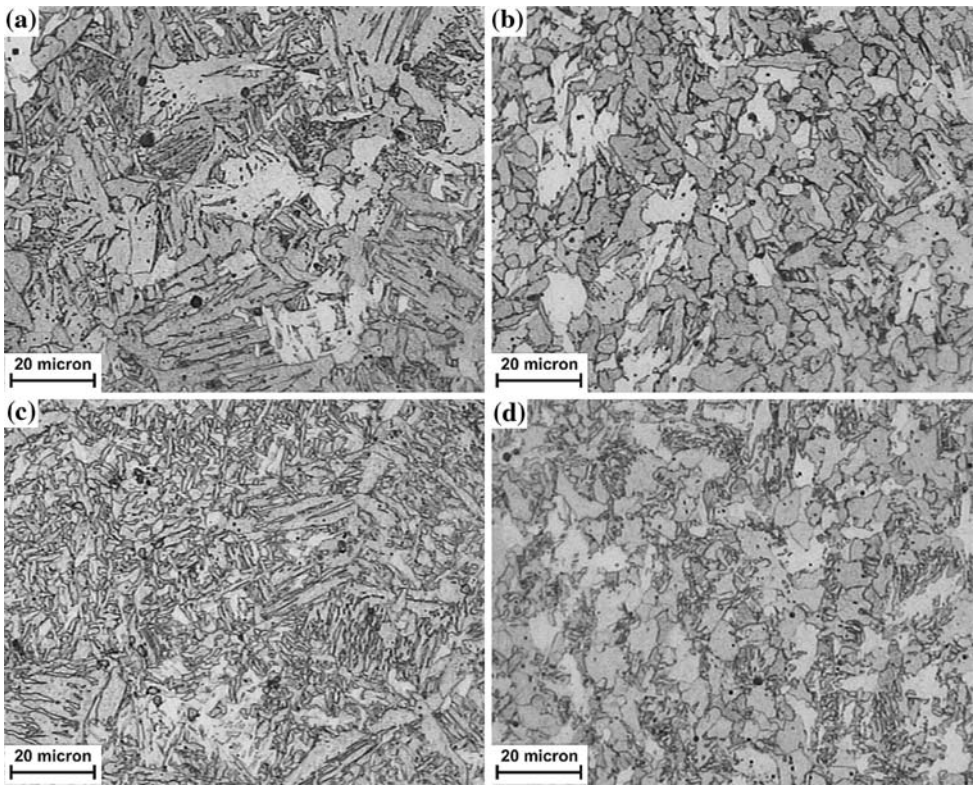

Fig. 4 Optical micrographs of reheated regions of last bead. **a** and **b** CGRZ and FGRZ of 0.05 wt% Cr, and **c** and **d** CGRZ and FGRZ of 0.91 wt% Cr in weld metal respectively

are shown in Fig. 4. Results of quantitative examinations are presented in Table 4.

Microstructure of CGRZ resembles that of the last bead, except for the columnar austenite grain structure that is replaced with equiaxed grains. Microstructural constituents are the same as those of columnar microstructure, but coarser in size. Like the last bead, in CGRZ, percentage of AF increases at the expense of PF and FS as the Cr content of the weld metal increases. Refinement of microstructure is also apparent, in Fig. 4a, c.

Microstructure of FGRZ is uniform at low levels of Cr and mainly consists of equiaxed ferrite grains with small amounts of microphases (dark etch contrasted in Fig. 4b). Increasing Cr content makes the microstructure nonuniform. It consists of some large equiaxed ferrite grains, with the rest being fine grain ferrite. As the Cr content increases the percentage of this fine ferrite increases.

Microphases

The Beraha tint etchants used in metallographic studies are: colored ferrite, pearlite, bainite, and martensite [20]. Sulfides are also brightened, while other microstructural constituents like austenite, remain unaffected. The color of phases is not constant on the whole surface of metallographic specimens; for example, the color of ferrite varies from orange to violet. We believe that the white phase observed in all of the microstructures of our experimental welds (Fig. 5), is retained austenite that has remained unaffected. This phase appears in the columnar, CGR, and FGR zones of each of as-deposited bead and fully or partially disappears or transforms to other constituents that have dark etch contrast in reheated beads (Fig. 5). Any constituent other than austenite should not disappear or transform to other constituents. Another possibility is that, the white phase is carbide. If it was carbide, it should only be tempered or spheroidized in subsequent heating cycles.

Based on the above, color metallography revealed that increasing chromium content of the weld metal increases the volume fraction of the white microphases in columnar, CGR, and FGR zones (Table 5 and Fig. 5). In the columnar zone of the welds with low Cr content, both dark- and white-etch contrasted microphases were seen. Percentage of dark microphase was negligible and was rarely seen in the vicinity of grain boundary allotriomorphs and between FS plates. Between AF plates, only white microphases were seen. With increasing Cr content, only the white microphases were seen in all the constituents (AF, FS, and PF). Both blocky and elongated morphologies of microphases were observed for all chromium levels.

In CGRZ produced by the last bead, percentage of white microphases increases with the increasing Cr content of weld metal. Percentage of white microphases is to some extent lower than that of columnar zone and dark microphases are simply seen in this region. This is because of

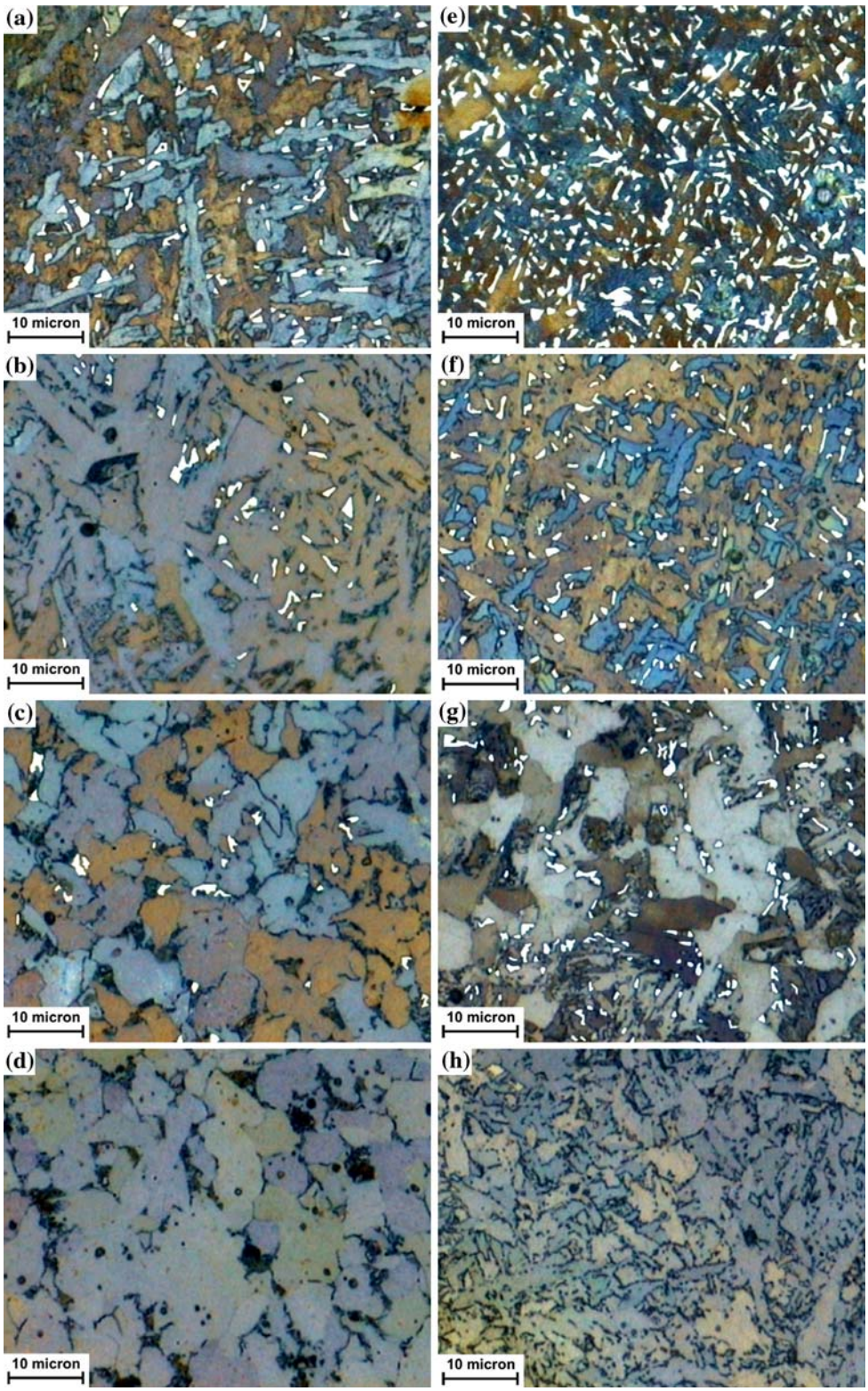

Fig. 5 Color optical micrographs showing change in microphases in different regions of weld metal for two extreme Cr contents, **a–d** columnar zone, CGRZ, FGRZ, and center of whole weld beads of specimen containing 0.05 wt% Cr, **e–h** columnar zone, CGRZ, FGRZ, and center of whole weld beads of specimen containing 0.91 wt% Cr

lower cooling rate in this zone as compared to that in columnar zone that permits austenite to transform more easily into other constituents. Another reason may be the smallness austenite grain size in this region. It has been demonstrated that larger austenite grains lower the $\gamma \rightarrow \alpha$ temperature, and thereby increase the fraction of the retained austenite [21]. Percentage of dark microphases decreases with increasing Cr content of the weld metal.

Table 5 Percentage of white microphases in different regions of weld metal

wt% Cr in weld metal	Columnar (%)	CGRZ (%)	FGRZ (%)
0.05	2.9	2.1	1.8
0.53	4.8	3.6	2.4
0.91	8.8	4.3	4.1

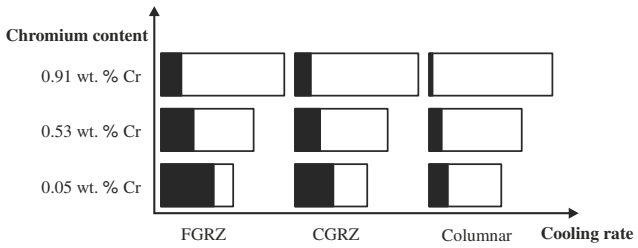

Fig. 6 Schematic diagram showing change in nature of microphases from dark to white with respect to both hardenability and cooling rate

The same trends as columnar and CGR zones can be seen in FGRZ produced by the last bead. Because of the lowest cooling rate and the smallest austenite grain size in this region, percentage of white microphases is lower and percentage of dark microphases is higher than that in the former regions. Exact determination of the nature of these dark microphases in reheated beads needs more detailed TEM study, because this could not be accomplished by this etching technique or SEM examination. The above described trends in change of the nature of microphases are shown schematically in Fig. 6. It should be noted that due to fineness of microphases, especially in high Cr contents, the dark microphases could not be easily distinguished from grain boundaries. Therefore, quantitative analysis of microphases was conducted only on white microphases.

Distribution of microphases is also altered as Cr level increases. With increasing Cr content, microstructure becomes more uniform (Table 4), and mainly consists of AF in both columnar and CGR zones. Distribution of microphases dispersed between different constituents also becomes more uniform and refined (Fig. 5).

Inclusions

Nonmetallic inclusions have two opposing effects. By providing an inert surface, they can assist the intra-granular nucleation of acicular ferrite that increases both strength and toughness [22–25], or they can be the initiation sites for both ductile and cleavage fracture [7, 26], depending on their chemistry and size. Distribution of inclusions is largely determined by solidification state, which in turn is a function of consumables and welding parameters [27].

Results of quantitative study of inclusions are presented in Table 6 and Fig. 7. Volume fraction of inclusions and some other statistical data are listed in Table 6. Some of these data such as volume fraction, apparent minimum, maximum, and average diameter, and number of counted inclusions are directly achieved from SEM images. Other data are calculated from stereological relations presented in [28]. These results do not show a general trend. It is clear that neither volume fraction, nor size distribution (Fig. 7), of nonmetallic inclusions are affected by variation of chromium content of the weld metal. Figure 7 also shows that the majority of inclusions have diameters in the range 0.1–1.0 μm.

The chemical composition of inclusions was not affected by chromium content of weld metal. Chemical analysis of some inclusions showed similar constituents in different samples. Major elements are: titanium, manganese, silicon, oxygen, and minor constituents are: aluminum (rarely detected) and sulfur. Because of the complex and multi-phase nature of inclusions, it is difficult to find out their true nature through EDS analysis without more supplementary analytical studies. However, according to [24, 25, 29, 30], it could be claimed that the phases are a Ti-rich oxide phase, $MnOSiO_2$, and MnS. A typical EDS spectrum of an inclusion of a specimen containing 0.53 wt% Cr is shown in Fig. 8.

These results indicate that chromium does not significantly affect the nonmetallic inclusions. This finding consistent with results reported by other researchers [31]. These results also confirm that volume fraction of nonmetallic inclusions is strongly dependent on the level of oxygen and sulfur of the weld metal. Since oxygen and

Table 6 Results of quantitative metallography for nonmetallic inclusions

wt% Cr in weld metal	f (%)[a]	D_{min} (μm)[a,b]	D_{max} (μm)[a]	$\bar{D}_{app.}$ (μm)[a]	$\bar{D}_{true}$ (μm)[a]	N[a]	N_V (mm^{-3})[a]	X_0 (μm)[a]
0.05	0.5	0.2	2.2	0.489	0.335	681	34196.000	17.07
0.53	0.4	0.1	1.9	0.451	0.305	739	40739.656	16.10
0.91	0.5	0.1	1.8	0.539	0.351	571	27361.168	18.38

[a] Parameters used above are: f, inclusion volume fraction; D_{min}, apparent minimum diameter; D_{max}, apparent maximum diameter; $\bar{D}_{app.}$, apparent average diameter; $\bar{D}_{true}$, true average diameter; N, number of counted inclusions; N_V, number of inclusions in unit volume; and X_0 is the inclusion spacing that is taken to be the average nearest-neighbor distance

[b] Inclusions with diameter less than 0.1 μm are intentionally excluded

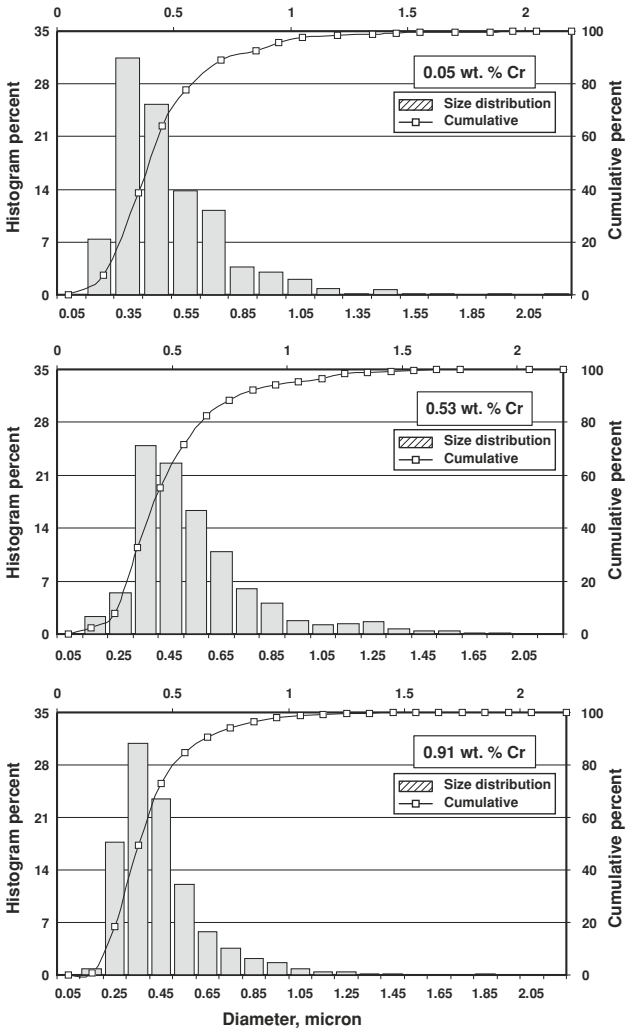

Fig. 7 Histogram of size distribution of inclusion as a function of Cr content in weld metal

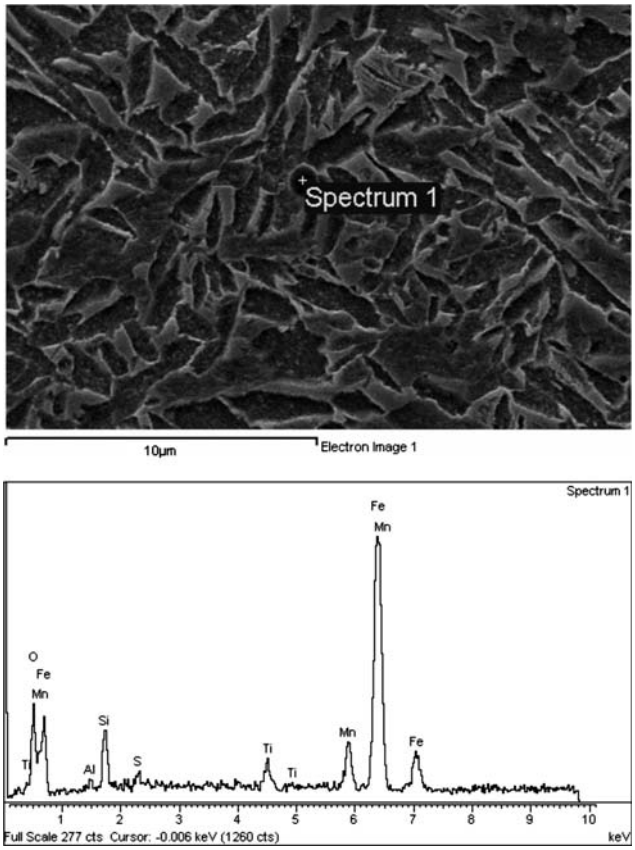

Fig. 8 Typical EDS spectrum from one inclusion of weld containing 0.53 wt% Cr

sulfur content of the weld metal are fairly constant in our experiments, it is acceptable that volume fraction of inclusions remain constant too.

Mechanical testing

Hardness testing

Horizontal hardness profile from specimen containing 0.53 wt% Cr, starting from base toward weld metal are presented in Fig. 9. A uniform increase in hardness from base metal to HAZ, and then to weld metal can be seen in this figure. This may be due to the changes in microstructure, and both microstructure and chemical composition in HAZ and weld-metal respectively.

The hardness profiles achieved from the all-weld metal as a function of Cr content are presented in Fig. 10. It can be seen that the hardness increases as Cr content of weld metal increases. The effect is less pronounced for 0.53 and 0.91 wt% Cr especially in the reheated beads.

Chromium can increase hardness by solid solution hardening, precipitation of hard phases like carbides, promotion of harder phases like AF instead of PF in this case, and refinement of microstructure. Chromium dissolves in ferrite without limit, and its main effect on mechanical properties is through solid solution hardening. Table 4 shows that it also increases percentage of AF which is harder than PF or FS. The precipitation of hard phases needs additional evaluation with TEM.

Tensile properties

Results of tensile tests as a function of Cr content of the weld metal are presented in Table 7 and Fig. 11. Both yield and ultimate tensile strengths increase and elongation decreases with increasing Cr content of the weld metal. The tensile test results are in agreement with hardness results, and similarly, incremental trend slow down for the samples containing 0.53 and 0.91 wt% Cr. Therefore,

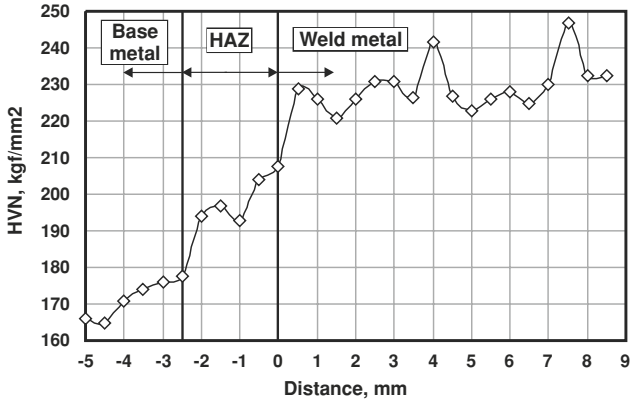

Fig. 9 Hardness profile from base-metal to weld-metal (Vickers method with 1-kg force)

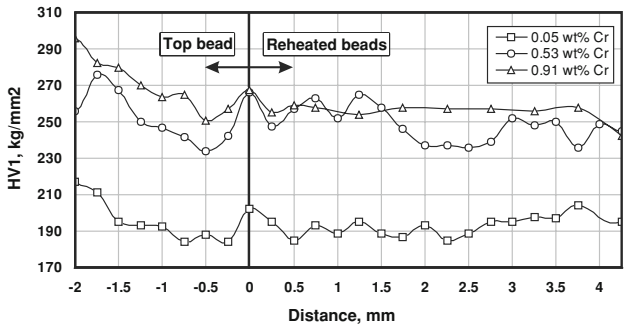

Fig. 10 Hardness profiles with 1-kg force, started from top bead toward the reheated regions

similar variation of tensile properties with increasing Cr content follows similar arguments as for hardness.

SEM micrographs of fracture surfaces of tensile specimens are shown in Fig. 12. The fracture surfaces show features of fully ductile fracture. On the fracture surface of 0.91 wt% Cr, number of cracks can be seen. Size of dimples seems to be the same in both micrographs.

Charpy impact toughness

Results of impact tests for each specimen are listed in Table 7 and shown in Fig. 13. A slight increase in Charpy-absorbed energy with increasing Cr content can be seen in this figure. There are several parameters affecting impact toughness of welds including

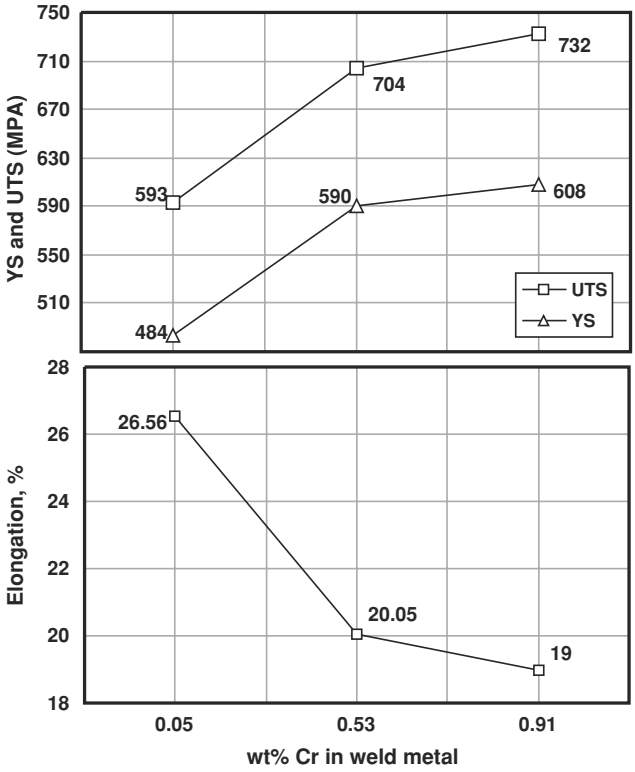

Fig. 11 Tensile properties as a function of wt% Cr in weld metal

1. hardness (or strength) level,
2. microstructure (percentage of different regions in Charpy notch location),
3. inclusions characteristics like volume fraction of inclusions, size and spacing, and
4. percentage of MAC.

In general, toughness decreases with increasing hardness (or strength), because the ability of material for plastic deformation decreases, and hence work of fracture decreases. Although some microstructural constituents like AF have higher strength and hardness than other ferrite morphologies their impact toughness is also higher [8–10, 32]. Allotriomorph ferrites show little resistance to cleavage fracture and have low impact toughness especially at low temperatures [7]. Microstructures like FS or bainite

Table 7 All-weld metal tensile properties and Charpy absorbed energy

wt% Cr in weld metal	Tensile properties			Charpy absorbed energy	
	YS	UTS	El.	Discrete values	Average value
0.05	484	593	26.56	49, 40, 40, 34	40
0.53	590	704	20.05	46, 42, 42, 40, 38	41.33
0.91	608	732	19	48, 42, 42, 36	42

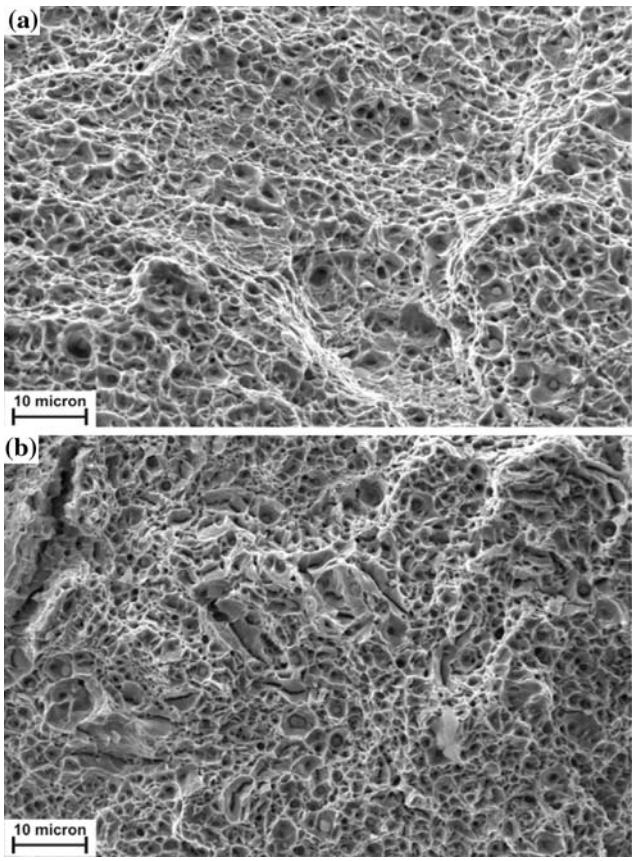

Fig. 12 SEM micrograph of fractured surfaces of tensile, **a** 0.05 wt% and **b** 0.91 wt% Cr content

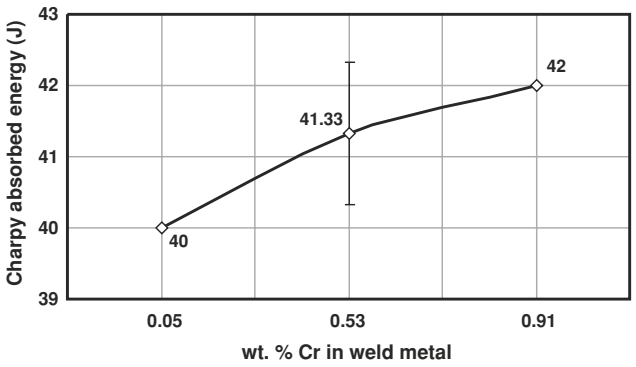

Fig. 13 Charpy impact energy as a function of Cr content of weld metal

that have parallel plates with low angle boundaries also have low impact toughness.

Different regions of the weld metal have different impact toughness, but in this case, contradicting results have been reported [11, 33]. Amongst weld regions, columnar region seems to have inferior toughness as compared with reheated regions. According to Jorge et al. [11], as the fraction of reheated regions in Charpy notch location increase, impact toughness decreases. However, opposite results have been presented by [33] claiming that the effect of the proportion of different regions—i.e., fraction of columnar and reheated regions in Charpy V-notch location—is negligible.

Inclusions have two opposite effects on mechanical properties of welds. If they do not provide efficient sites for nucleation of AF, they are detrimental to toughness. In this respect volume fraction, especially for inclusions greater than 1 μm in diameter [26, 33, 34], size, spacing and their resistance to void nucleation must be considered.

MAC is an important factor in controlling toughness. This phase has two morphologies, namely elongated and blocky shapes. Elongated MAC can crack under load and blocky MAC can induce stress in adjacent phase, if it is a ductile phase such as ferrite [7]. This phase is detrimental to toughness especially at low temperatures. It has been reported that there is a direct relationship between toughness and percentage of MAC; that is, increase in MAC leads to decrease in toughness [11].

In our case, however, all of these parameters are either constant or they have no correlation to toughness. By precise metallographic examination of notch location, it was found that as percentage of microphases increases with chromium content of the weld metal, morphology of these microphases also changes, especially in reheated beads. Figures 5 and 6 show that increasing chromium content changes the nature of microphases from dark for low chromium content to almost all white—i.e., retained austenite—for high chromium content in all columnar, CGR, and FGR zones. These microphases become finer and their distribution becomes more uniform throughout microstructure. It may be concluded that this retained austenite decomposes in subsequent heating cycles of overlying beads to dark microphases that also are finer in size and more uniform in distribution. Then, during welding of the following layers, these dark microphases temper and their carbides become spherical. The carbides in low chromium content samples are also partially spheroidized. Their distribution is nonuniform and localized, and appears in distinct large islands. This behavior is shown in Fig. 14. Change in the kinetics of spheroidizing of carbides may be due to change in the nature of dark microphases from diffusional (e.g., ferrite-carbide aggregate) in low chromium content to displacive products (e.g., bainite or martensite) in high chromium content.

Summary

Effect of chromium additions to low alloy steel weld metal deposits in the range of 0.05–0.91 wt% were studied. It is found that as the chromium content of the weld metal increases:

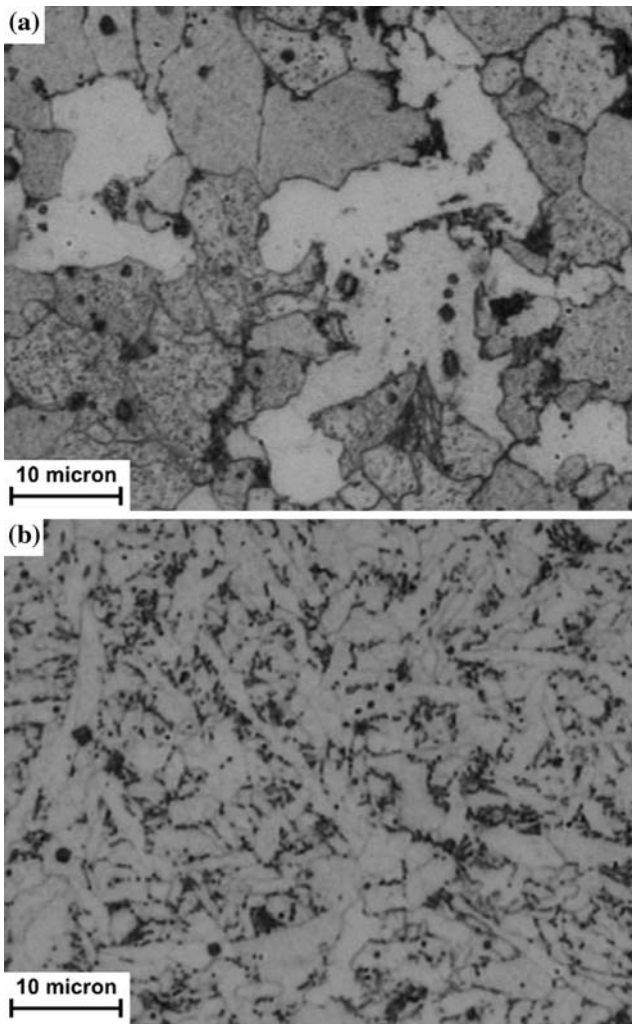

Fig. 14 Optical micrographs showing spheroidizing of carbides in notch location of **a** 0.05 wt% and **b** 0.91 wt% chromium content

1. Amount of AF increases uniformly at the expense of other constituents in both columnar and CGR zones.
2. Microstructure becomes finer in all zones of welding.
3. Percentage of microphases increases uniformly in all regions. The tint etchants used show many useful data that all can be achieved with optical microscopy.
4. Chromium does not affect nonmetallic inclusions in a significant way.
5. Hardness and similarly tensile properties increase mainly because of solid solution hardening effect of chromium. Promotion of hard phases and refinement of microstructure are also operative.
6. Charpy V-notch impact toughness also increases because of fine dispersed spheroidized dark microphases in high Cr levels.

Acknowledgements The authors are grateful to Mr. Kargozar, the deputy, and Mr. E. Abbasi, the research manager of "*JVOC*" for fabrication of laboratory electrodes and preparing all the samples. Mr. Avazkonandeh also thanks "*Nahamin Pardazan Asia Co*." for support in quantitative metallography.

References

1. Bhadeshia HKDH, Svensson LE, Gretoft B (1985) Acta Metall 33:1271
2. Bhadeshia HKDH, Svensson LE (1993) In: Cerjak H, Easterling KE (eds) Mathematical modeling of weld phenomena. Institute of Materials, London
3. Kou S (2003) Welding metallurgy. John Wiley & Sons, New Jersey
4. Esterling KE (1985) Introduction to physical metallurgy of welding. Butterworths, London
5. Bhadeshia HKDH, Svensson LE, Gretoft B (1986) J Mater Sci 21:3947. doi:10.1007/BF02431634
6. Honeycombe RWK, Bhadeshia HKDH (2006) Steels. Butterworth-Heinemann Publications, Oxford
7. Bhadeshia HKDH (1997) In: Cerjak H, Bhadeshia HKDH (eds) Mathematical modeling of weld phenomena III. Institute of Materials, London
8. Yang JR, Huang CY, Huang CF et al (1993) J Mater Sci Lett 12:1290
9. Byun JS, Shim JH, Suh JY et al (2001) Mater Sci Eng A 319–321:326
10. Ohkita S, Horii Y (1995) ISIJ Int 35:1170
11. Jorge JCF, Souza LFG, Rebello JMA (2001) Mater Charact 47:195
12. Jorge JCF, Souza LFG, Rebello JMA et al (2000) IIW doc. II-1398-00
13. Surian ES, De-Vedia LA (1999) Welding J 78:217s
14. ANSI/AWS A5.5-96, Specification for low alloy steel electrodes for shielded metal arc welding. American Welding Society, Miami, 1996
15. Bradley JR, Aaronson HI (1981) Metall Trans A 12:1729
16. Beche A, Zurob HS, Hutchinson CR (2007) Metall Mater Trans A 38:2950
17. Shiflet GJ, Aaronson HI, Bradley JR (1981) Metall Trans A 12:1743
18. Babu SS (2004) Curr Opin Solid State Mater Sci 8:267
19. Farrar RA, Harrison PL (1987) J Mater Sci 22:3812. doi:10.1007/BF01133327
20. Vander Voort GF (1992) Metals handbook, vol 9. ASM Int., Ohio
21. Harrison PL, Farrar RA (1981) J Mater Sci 16:2218. doi:10.1007/BF00542384
22. Bhadeshia HKDH (2001) Bainite in steels. IOM Comunications Ltd., London
23. Lee TK, Kim HJ, Kang BY et al (2000) ISIJ Int 40:1260
24. Court SA, Pollard G (1989) Metallography 22:219
25. St-Laurent S, L'Esperance G (1992) Mater Sci Eng A 149:203
26. Tweed JH, Knott JF (1987) Acta Metall 35:1401
27. Sugden AB, Bhadeshia HKDH (1988) Metall Trans A 19:669
28. Garrison WM Jr, Wojcieszynski AL (2007) Mater Sci Eng A 464:321
29. Bose-Filho WW, Carvalho ALM, Strangwood M (2007) Mater Charact 58:29
30. Shim JH, Oh YJ, Suh JY et al (2001) Acta Mater 49:2115
31. Dowling JM, Corbett JM, Kerr HW (1986) Metall Trans A 17:1611
32. Sugden AB, Bhadeshia HKDH (1988) Metall Trans A 19:1597
33. Powell GLF, Herfurth G (1998) Metall Mater Trans A 29:2775
34. Ishikawa T, Haze T (1994) Mater Sci Eng A 176:385